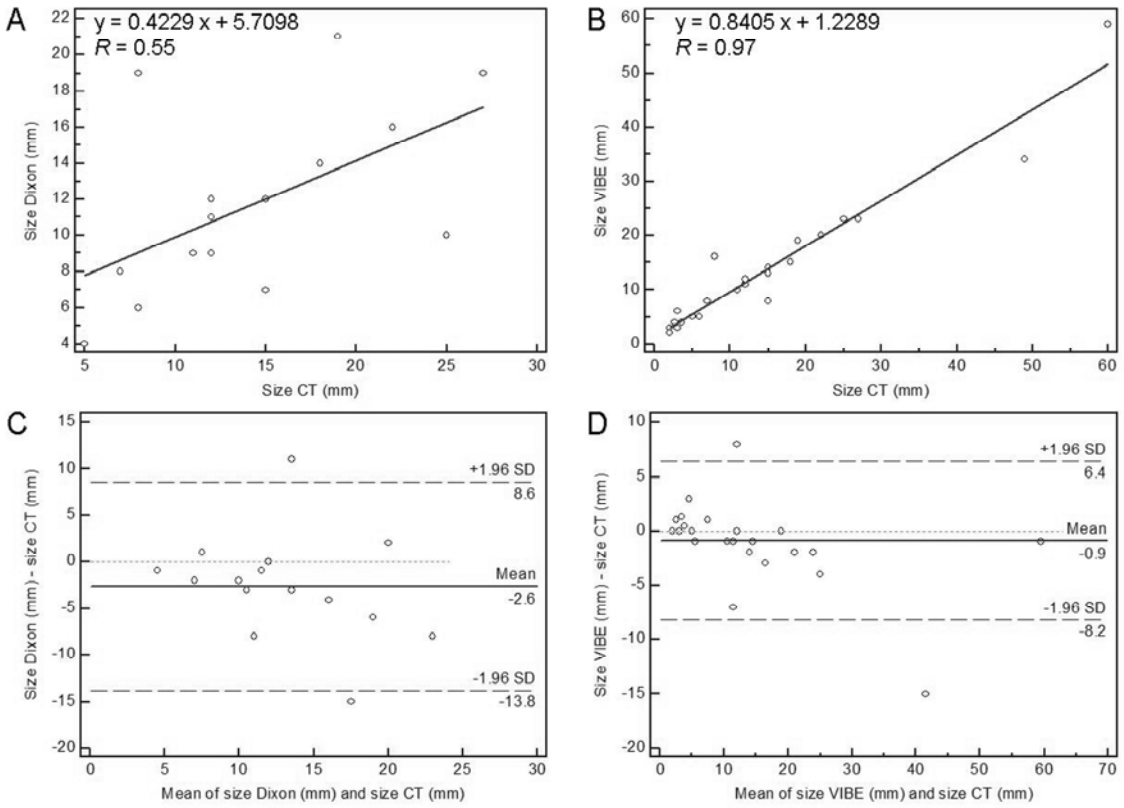

Supplemental Figure 1: Correlation analysis of lesion size between CT and Dixon (A) and VIBE (B). X-axis displays mean size of lung lesion as obtained by CT, and y-axis displays corresponding values by Dixon and VIBE sequence. High correlations as expressed by the Spearman correlation coefficient (*R*) are found between lesion size in CT and VIBE (*R* = 0.97) and between CT and Dixon (*R* = 0.55).

The difference between the two size measurement is shown by the Bland–Altman (C for lesion size in Dixon and D for lesion size in VIBE) on which the difference between 2 SUV measurements is plotted against their average: For lesion size Dixon mean difference is -2.6 mm; the 95% CIs are +8.6 and -13.8 mm, for lesion size VIBE the mean difference is -0.9 mm; the 95% CIs are +6.4 and -8.2 mm.

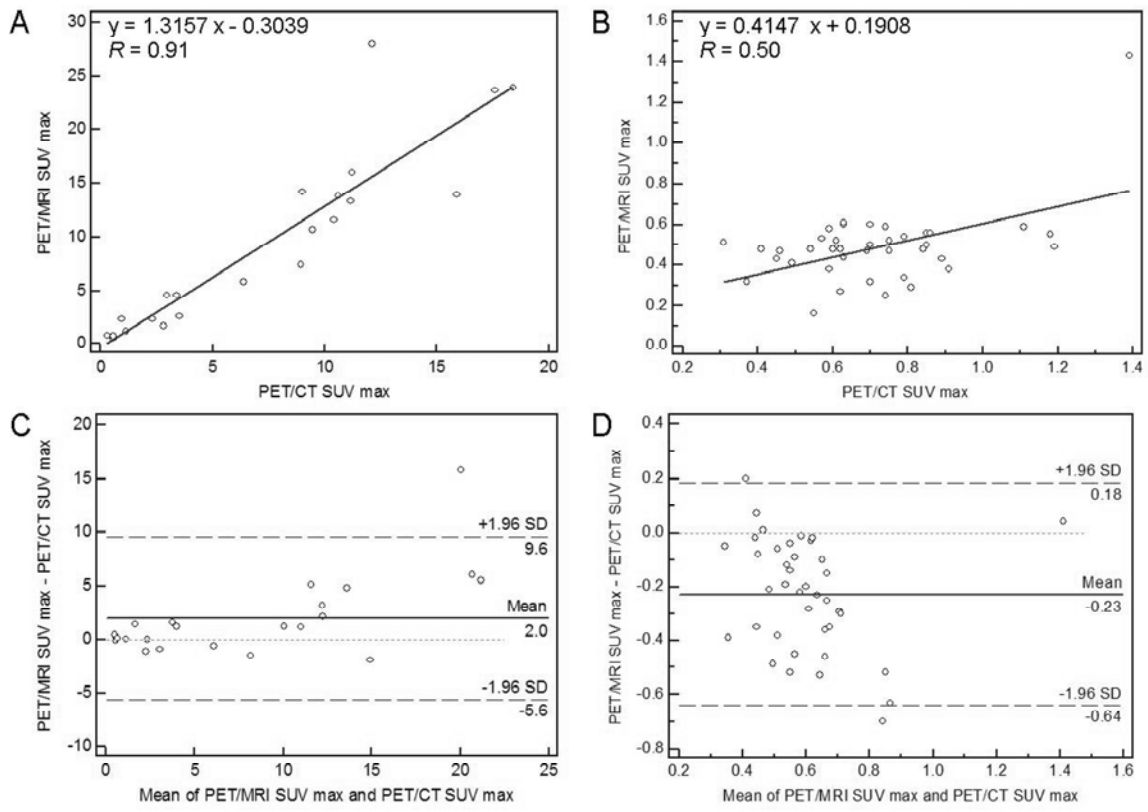

Supplemental Figure 2: Correlation analysis of tracer uptake between PET/CT and subsequent PET/MR as assessed by SUV_{max} in lung lesions (A) and normal lung parenchyma (B). X-axis displays quantitative values as obtained by PET/CT, and y-axis displays corresponding values by PET/MR. High correlations as expressed by the Spearman correlation coefficient (*R*) are found for SUV_{max} (*R* = 0.50 for normal lung parenchyma, *R* = 0.91 for lung lesions) between findings from both modalities.

The difference between the two SUV measurement is shown by the Bland–Altman (C for SUV_{max} in lung lesions and D for SUV_{max} in the normal lung parenchyma) on which the difference between 2 SUV measurements is plotted against their average: For $SUV_{max\text{-}healthy\ lung}$ the mean difference is -0.23 SUV; the 95% CIs are +0.18 and -0.64 SUV, for $SUV_{max\_lung\ lesion}$ mean difference is +2.0 SUV; the 95% CIs for SUV_{max} are +9.6 and -5.6 SUV.

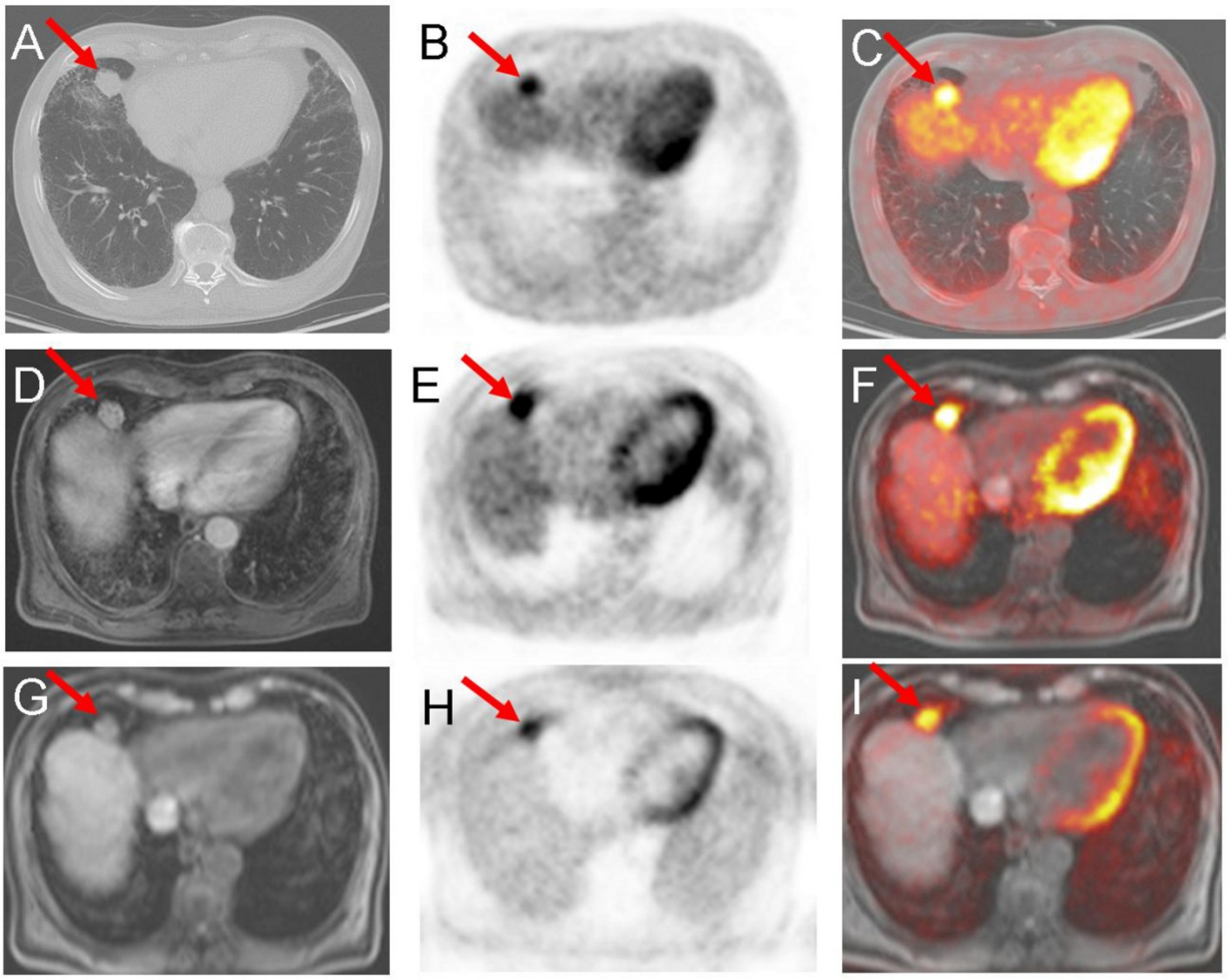

Supplemental Figure 3: 78-year old patient with bronchial carcinoma and a lung metastasis which was [^{18}F]FDG positive and was seen in CT and both VIBE and Dixon sequence. Figure A, D and G show morphological datasets (A axial CT, D axial VIBE, G axial Dixon sequence). Figure B, E and H show the corresponding PET datasets (B PET of PET/CT, E PET AC of PET/MR, H PET NAC of PET/MR). The corresponding fusioned PET/CT is shown in Figure C, the fusioned PET/MR in F (fusion of VIBE with PET) and I (fusion of Dixon with PET).

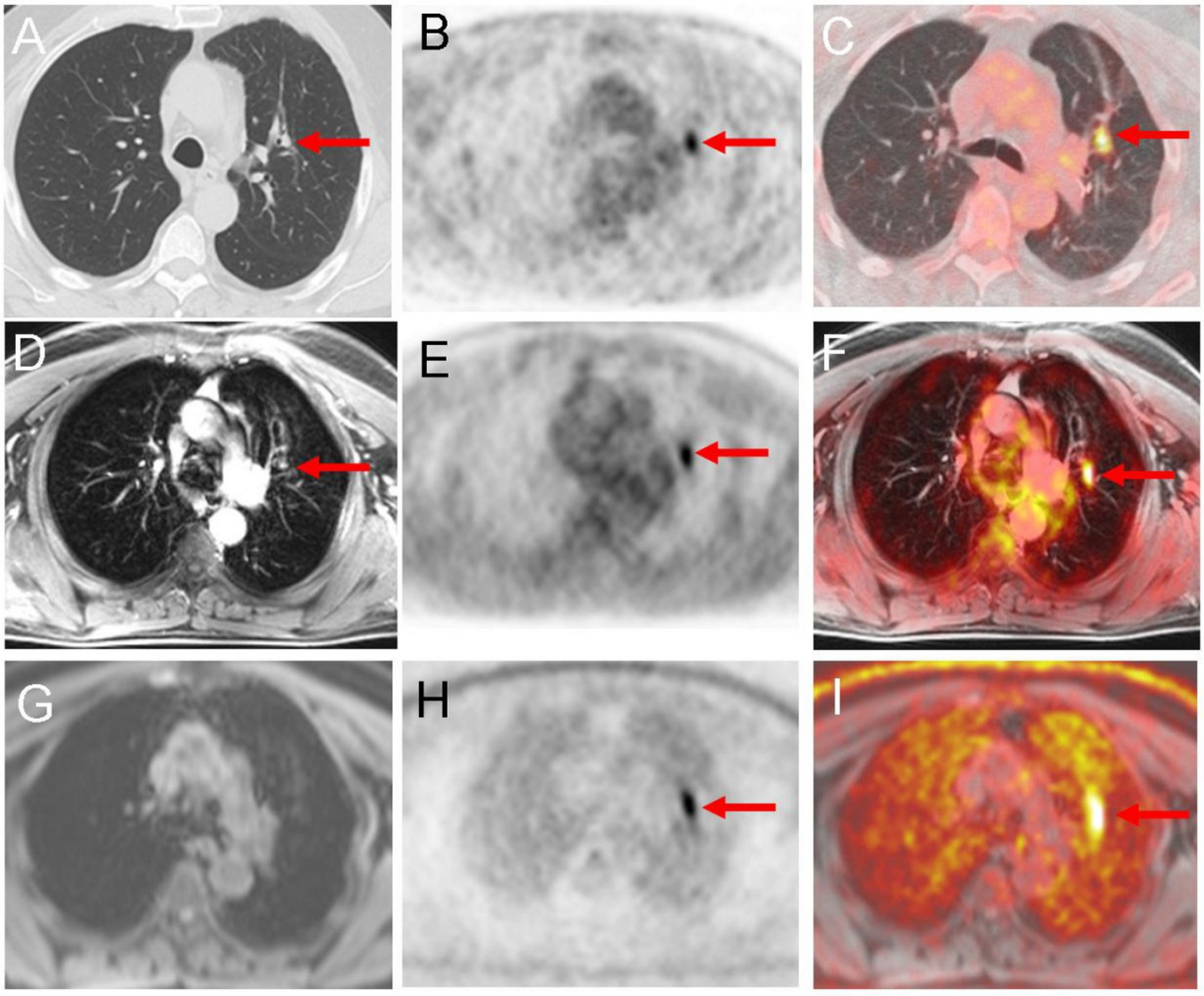

Supplemental Figure 4: 66-year old patient with thyroid cancer and a lung metastasis which was [^{18}F]FDG positive and was seen in CT and VIBE but not in the Dixon sequence. Figure A, D, G and I show morphological datasets (A axial CT, D axial VIBE, G and I axial Dixon sequence). Figure B, E and H show the corresponding PET datasets (B PET of PET/CT, E PET AC of PET/MR, H PET NAC of PET/MR). The corresponding fusioned PET/CT is shown in Figure C, the fusioned PET/MR in F (fusion of VIBE with PET).

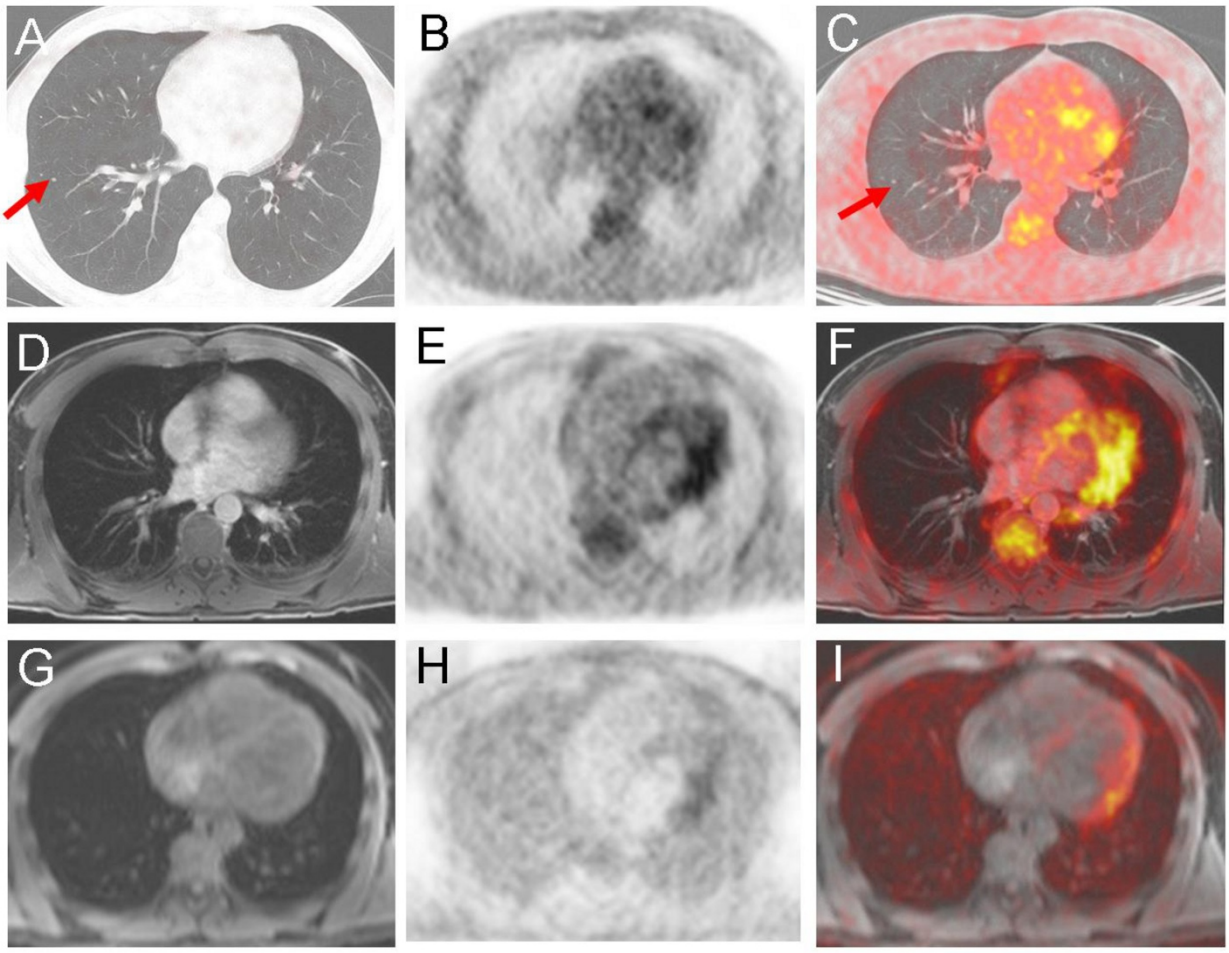

Supplemental Figure 5: 41-year old patient with thyroid cancer and a lung metastasis (4 mm diameter) which showed no suspicious [^{18}F]FDG uptake and was seen in CT but not in the Dixon and VIBE sequence. Figure A, D, G and I show morphological datasets (A axial CT, D axial VIBE, G and I axial Dixon sequence). Figure B, E and H show the corresponding PET datasets (B PET of PET/CT, E PET AC of PET/MR, H PET NAC of PET/MR). The corresponding fusioned PET/CT is shown in Figure C, the fusioned PET/MR in F (fusion of VIBE with PET).